Effect of functional on the absorption of CO and CO_2 on Silicon-doped Boron-nitride Nanosheet

Md. Humaun Kabir*, Md. Alamgir Badsha

Department of Physics, Jashore University of Science and Technology, Jashore 7408, Bangladesh.
Email: mhkabir@just.edu.bd, alamgir93_phy@just.edu.bd
*Corresponding Author: mhkabir@just.edu.bd

Abstract:
Hybrid density functional play a vital role in density functional theory (DFT) calculations. CO and CO_2 gases are toxic gases in the environment. Using first-principles within DFT, the effects of the hybrid density functionals MPW1PW91 and B3LYP on the adsorption performance of CO and CO_2 gases on Si-decorated Boron-nitride (SiBN) nanosheets are studied. Energy gaps and adsorption energies have been calculated to know the adsorption performance of CO and CO_2 by utilizing MPW1PW91 and B3LYP hybrid density functionals at 6-31G level. The results show that, the adsorption performance changes if the functional is changed. It was found that, sensing performance improves for CO while degrades for CO_2 as we change the functional from MPW1PW91 to B3LYP. The results indicate that for all the complexes, energy gaps decrease as we move from the functional MPW1PW91 to B3LYP.

Keywords— *Boron-nitride nanosheet; gas sensor; DFT, basis set, gas sensor, density functional.*

I. Introduction

The B3LYP technique utilizes Becke's three-parameter functional and the nonlocal correlation of Lee, Yang and Parr [1], [2]. The MPW1PW91 technique adopts Barone and Adamo's Becke-style one-parameter functional, the changed Perdew-Wang exchange and the Perdew-Wang 91 correlation [3], [4]. The performance of hybrid exchange functionals has been studied for presenting the characteristics of cubic and tetragonal ferroelectric phases of $BaTiO_3$ [5].

Resulting from partial oxidation and/or combustion of fuel, carbon monoxide (CO) is a key contributor for the pollution of the environment [6], [7], [8], [9], [10]. The atmospheric CO coming into the interaction with the heme of the human body, may result in a reduction in oxygen transfer mechanism and eventually may die. Carbon dioxide (CO_2) is utilized in the beverage production, manufacture of carbonates, CO, carboxylic acids, petroleum processes, and fertilizer production. Greenhouse effects are the main cause of CO_2 gas [11].

In this manuscript, we investigated the adsorption mechanism of CO and CO_2 gas molecules on the surface of SiBN nanosheet using the well known DFT study. The manuscript is organized as follows: in Section II, computational methods are discussed, results and discussions are placed in Section III, and Section IV describes the conclusions of the work.

II. Computational Methods

Adsorption of CO and CO_2 gas molecules on SiBN nanosheets has been investigated using first principles within DFT. The optimum structural parameters such as energy of adsorption, HOMO-LUMO energy gaps etc. are calculated. For the optimizations of the geometry, we use DFT computation at basis set 6-31G with B3LYP and MPW1PW91 functionals as implemented in Gaussian 09 program [12], [13], [14] [15]. Geometry optimizations and calculations of the property on Si–doped BN nanostructers with and without X molecule (X = CO, CO_2) are performed. The adsorption energies (E_{ads}) of X molecules with SiBN were calculated separately, using the following equation [16]:

$$E_{ads\,(SiBN)} = E_{X\text{-}SiBN} - (E_{SiBN} + E_X) \tag{1}$$

where $E_{ads(SiBN)}$ corresponds to the energies of interaction of X molecule with SiBN. $E_{X\text{-}SiBN}$ is total electronic energy of SiBN complex with analytes X, and E_X is the entire energy of a secluded X molecule. The HOMO and LUMO energies are used for determining the energy gap (E_g), as follows [17]:

$$E_g = E_{LUMO} - E_{HOMO}$$

(2)

SiBN: top view

SiBN-CO: top view

SiBN: side view

SiBN-CO: side view

(a)

(b)

SiBN-CO$_2$: top view

SiBN-CO$_2$: side view

(c)
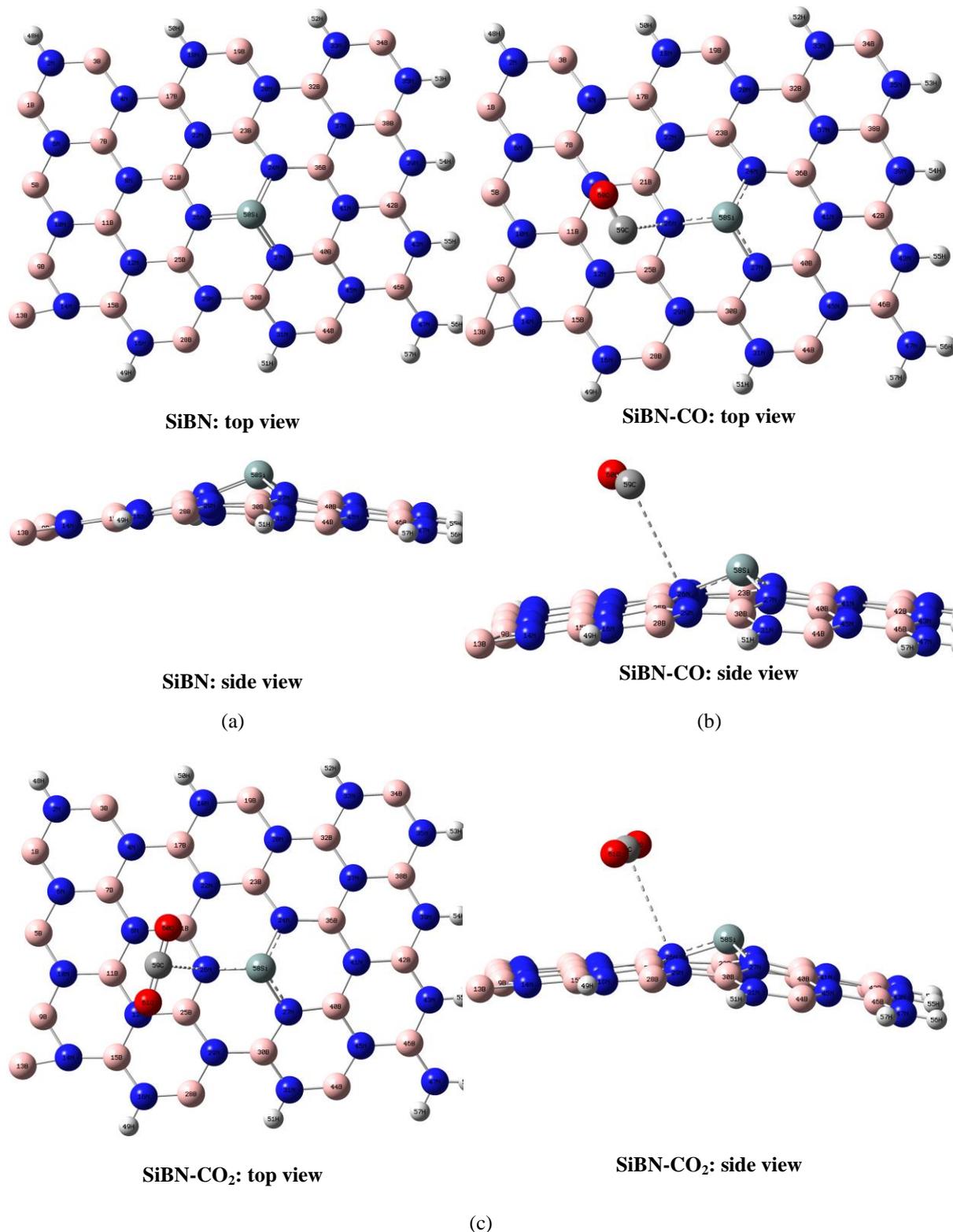
Figure 1. side and top views of (a): SiBN, (b) SiBN-CO, and (c) SiBN-CO$_2$ optimized structures as B3LYP/6-31G.

III. Results And Discussions

Optimized Geometric Structure

Side and top views of the optimized geometric configuration of bare SiBN, SiBN–CO, and SiBN–CO_2 are shown in Figure 1 and 2. Figure 1 corresponds to B3LYP/6-31G level and Figure 2 corresponds to corresponds to MPW1PW91/6-31G level.

Adsorption Energy (E_{ads})

E_{ads} at B3LYP Functional:

For the functional B3LYP, the pristine SiBN nanosheet interacts with CO and CO_2 with interaction energies of -3.344 kJmol^{-1} and -5.731 kJmol^{-1}, respectively (Table 1) [15].

E_{ads} at MPW1PW91 Functional:

For the functional MPW1PW91, the pristine SiBN nanosheet interacts with CO and CO_2 with interaction energies of -61.244 kJmol^{-1} and -0.960 kJmol^{-1}, respectively (Table 2). Unlike CO_2, adsorption performance improves for CO as we change the basis set from B3LYP to MPW1PW91.

SiBN: top view   SiBN-CO: top view

SiBN: side view   SiBN-CO: side view

(a)   (b)

SiBN-CO$_2$: top view

SiBN-CO$_2$: side view

(c)
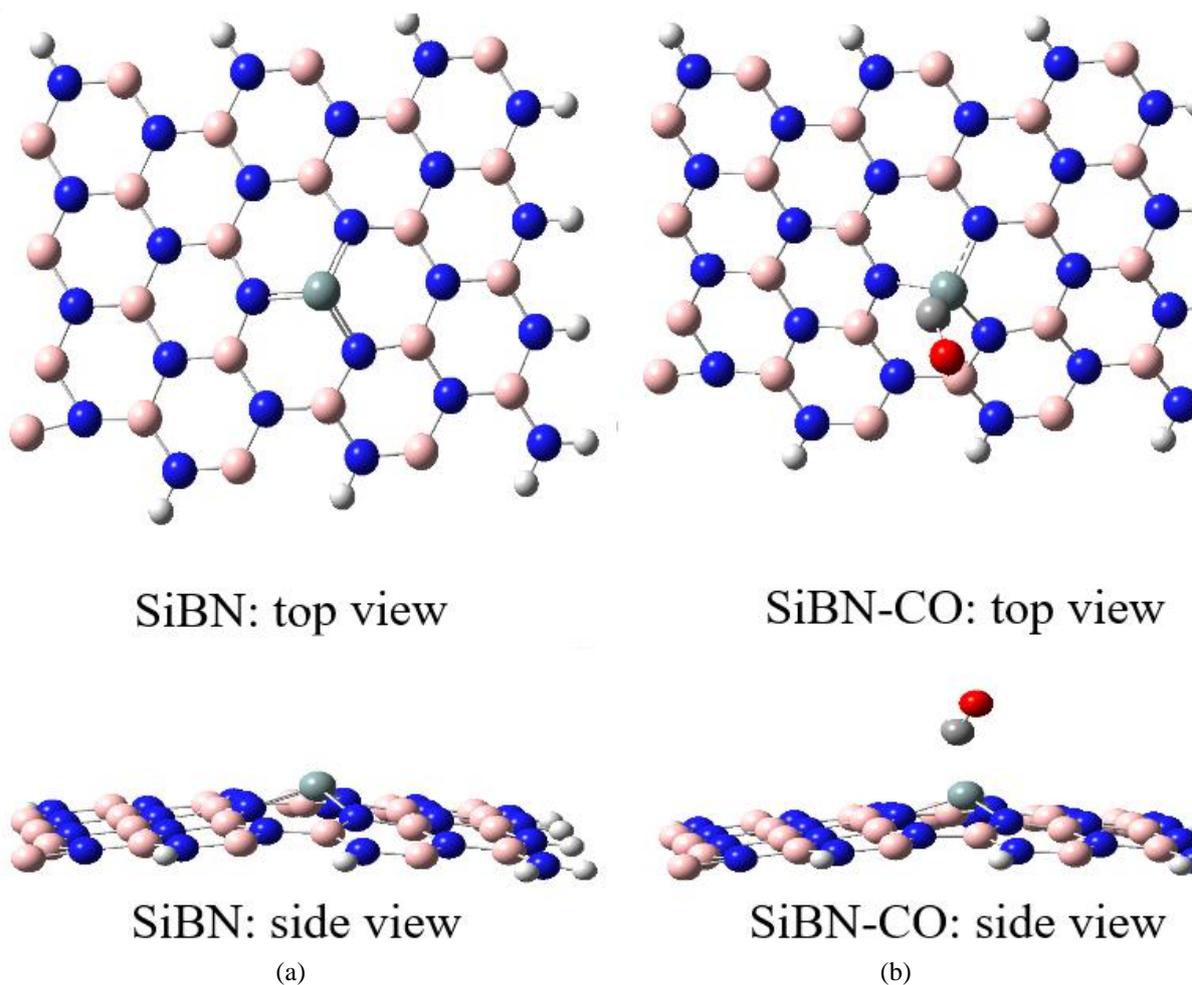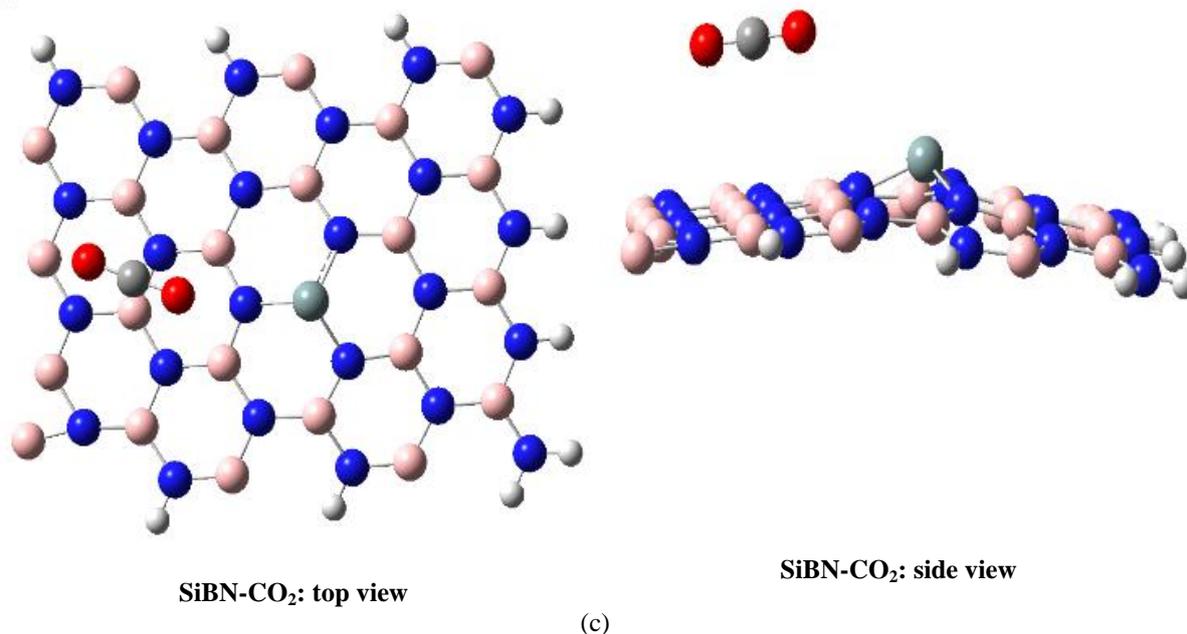
Figure 2. Top and side views of (a): SiBN, (b) SiBN-CO, and (c) SiBN-CO$_2$ optimized structures as MPW1PW91/6-31G

Table 1. HOMO Energy (E$_{HOMO}$), LUMO Energy (E$_{LUMO}$), HOMO-LUMO Energy Gap (E$_g$), and Adsorption Energy (E$_{ads}$) at B3LYP/6-31G Level [15]

System/ Properties	E$_{HOMO}$ (eV)	E$_{LUMO}$ (eV)	E$_g$ (eV)	E$_{ad}$ (kJmol^{-1})
CO	-10.108	-0.593	9.515	-
CO$_2$	-10.067	-0.814	9.254	-
SiBN	-4.871	-1.610	3.260	-
SiBN-CO	-4.893	-2.206	2.687	-3.344
SiBN-CO$_2$	-4.872	-2.225	2.647	-5.731

Table 2. HOMO Energy (E$_{HOMO}$), LUMO Energy (E$_{LUMO}$), HOMO-LUMO Energy Gap (E$_g$), and Adsorption Energy (E$_{ads}$) at MPW1PW91/6-31G Level

System/ Properties	E$_{HOMO}$ (eV)	E$_{LUMO}$ (eV)	E$_g$ (eV)	E$_{ad}$ (kJmol^{-1})
CO	-10.501	-0.855	9.646	-
CO$_2$	-10.538	0.206	10.744	-
SiBN	-5.324	-1.153	4.171	-
SiBN-CO	-5.370	-1.639	3.731	-61.244
SiBN-CO$_2$	-5.325	-2.387	2.938	-0.960

SiBN: HOMO

SiBN: LUMO

(a)

SiBN-CO: HOMO

SiBN-CO: LUMO

(b)

SiBN-CO$_2$: HOMO

SiBN-CO$_2$: LUMO

(c)
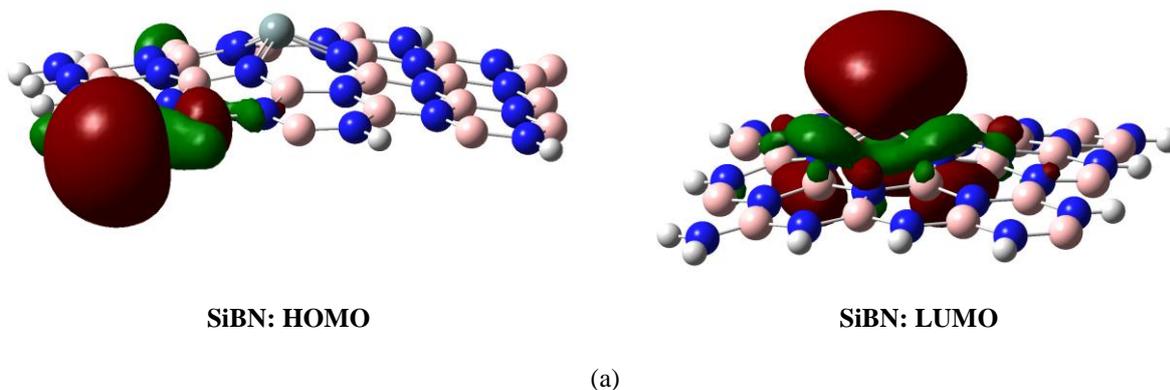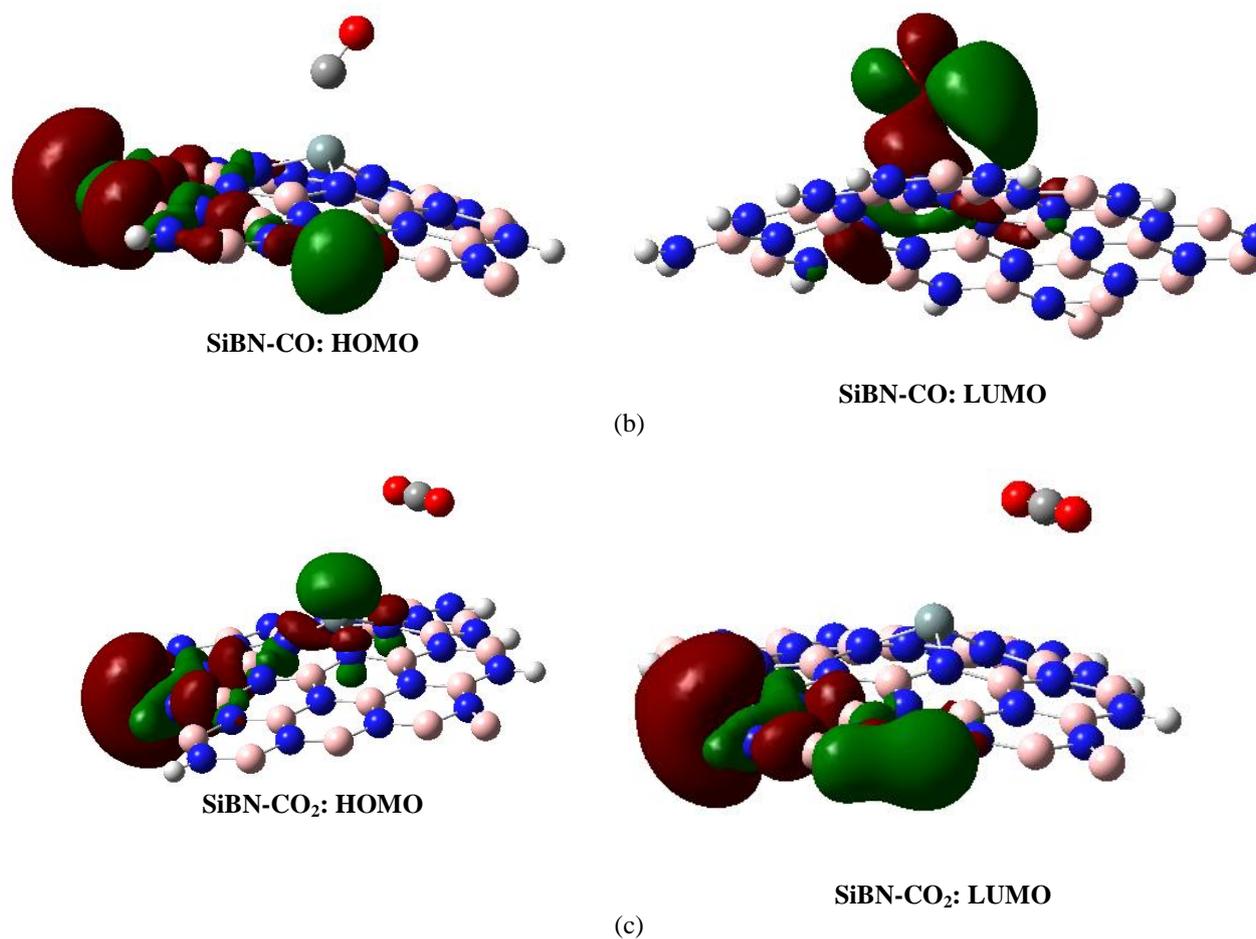
Figure 3. Molecular orbitals of HOMO and LUMO for (a) isolated SiBN, (b) SiBN-CO, and (c) SiBN-CO$_2$ at the B3LYP/6-31G level.

SiBN: HOMO

SiBN: LUMO

(a)

SiBN-CO: HOMO

SiBN-CO: LUMO

(b)

SiBN-CO$_2$: HOMO

SiBN-CO$_2$: LUMO

(c)
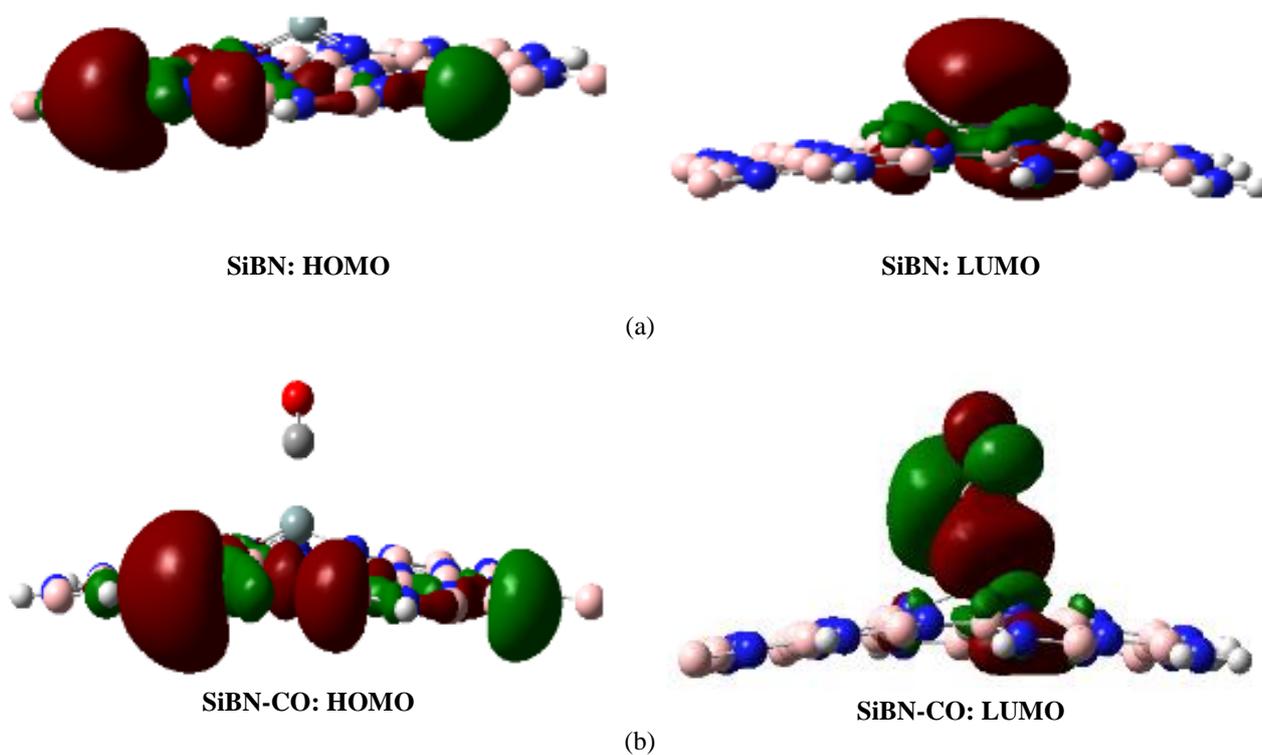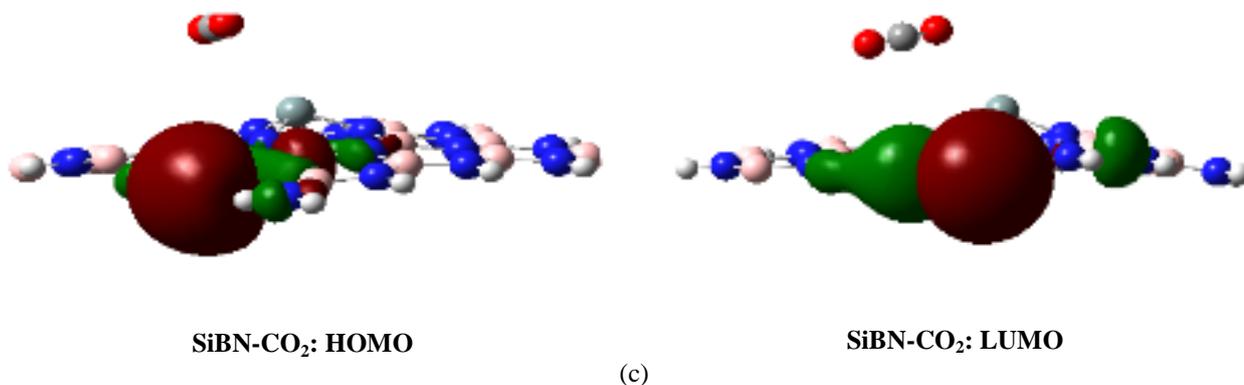
Figure 4. Molecular orbitals of HOMO and LUMO for (a) isolated SiBN, (b) SiBN-CO, and (c) SiBN-CO$_2$ at the MPW1PW91/6-31G level.

HOMO and LUMO Energy Gap (E$_g$)

E$_g$ at for functional B3LYP:
 HOMO and LUMO energy gaps for all the complexes for the functional B3LYP are shown in Table 1. The calculated HOMO-LUMO energy gap for SiBN nanosheet is 3.260 eV [15]. The HOMO-LUMO energy gap for SiBN-CO$_2$ complex is 2.647 eV compared to 2.687 eV for SiBN-CO complex [15].
The HOMO and LUMO energy distributions for the men-tioned systems at B3LYP/6-31G level are shown in Figure 3.

E$_g$ at Functional MPW1PW91:
 HOMO and LUMO energy gaps for all the complexes for the functional MPW1PW91 are shown in Table 2. The calculated HOMO-LUMO energy gap SiBN nanosheet is 4.171 eV. The HOMO-LUMO energy gap for SiBN-CO$_2$ complex is 2.938 eV compared to 3.731 eV for SiBN-CO complex. The HOMO and LUMO energy distributions for the mentioned systems at MPW1PW91/6-31G level are depicted in Figure 4.

The energy gap decreases for all the complexes if the basis set is changed from functional MPW1PW91 to B3LYP.

IV. Conclusions
 By utilizing first-principles within DFT, adsorption of CO and CO$_2$ gases on Si-decorated Boron-nitride nanosheets has been systemically investigated. Ad-sorption energies and HOMO-LUMO energy gaps are computed by utilizing DFT method at MPW1PW91 and B3LYP hybrid density functionals. The results indicate that for all the complexes, energy gaps decrease as we move from the functional MPW1PW91 to B3LYP. It was found that the adsorption performance changes if the functional is changed. However, unlike CO$_2$, adsorption performance improves for CO as we change the the functional from B3LYP to MPW1PW91. In our future studies, we will extend the research to other density functionals.
.

References
[1]. A. D. Becke, "Real-space post-hartree–fock correlation models," The Journal of chemical physics, vol. 122, no. 6, p. 064101, 2005.
[2]. T. Enevoldsen, J. Oddershede, and S. P. Sauer, "Correlated calcula-tions of indirect nuclear spin-spin coupling constants using second-order polarization propagator approximations: Soppa and soppa (ccsd)," Theoretical Chemistry Accounts, vol. 100, no. 5, pp. 275–284, 1998.
[3]. J. P. Perdew and Y. Wang, "Pair-distribution function and its coupling-constant average for the spin-polarized electron gas," Physical Review B, vol. 46, no. 20, p. 12947, 1992.
[4]. M. Hansen, M. Wendt, F. Weinhold, and T. Farrar, "Experimental and theoretical spin-spin coupling constants for [15n] formamide," Molecular Physics, vol. 100, no. 17, pp. 2807–2814, 2002.
[5]. F. Cora*,` "The performance of hybrid density functionals in solid state chemistry: the case of batio3," Molecular Physics, vol. 103, no. 18, pp. 2483–2496, 2005.

[6]. J. Beheshtian, M. T. Baei, and A. A. Peyghan, "Theoretical study of co adsorption on the surface of bn, aln, bp and alp nanotubes," Surface Science, vol. 606, no. 11-12, pp. 981–985, 2012.

[7]. T. Kjellstrom, M. Lodh, T. McMichael, G. Ranmuthugala, R. Shrestha, and S. Kingsland, "Air and water pollution: burden and strategies for control," in Disease Control Priorities in Developing Countries. 2nd edi-tion. The International Bank for Reconstruction and Development/The World Bank, 2006.

[8]. T.-M. Chen, W. G. Kuschner, J. Gokhale, and S. Shofer, "Outdoor air pollution: nitrogen dioxide, sulfur dioxide, and carbon monoxide health effects," The American journal of the medical sciences, vol. 333, no. 4, 249–256, 2007.

[9]. J. A. Raub, M. Mathieu-Nolf, N. B. Hampson, and S. R. Thom, "Carbon monoxide poisoning—a public health perspective," Toxicology, vol. 145, no. 1, pp. 1–14, 2000.

[10]. E. N. Allred, E. R. Bleecker, B. R. Chaitman, T. E. Dahms, S. O. Gottlieb, J. D. Hackney, M. Pagano, R. H. Selvester, S. M. Walden, and J. Warren, "Short-term effects of carbon monoxide exposure on the exercise performance of subjects with coronary artery disease," New England Journal of Medicine, vol. 321, no. 21, pp. 1426–1432, 1989.

[11]. H. Ullah, A.-u.-H. A. Shah, S. Bilal, and K. Ayub, "Dft study of polyaniline nh3, co2, and co gas sensors: comparison with recent experimental data," The Journal of Physical Chemistry C, vol. 117, no. 45, pp. 23 701–23 711, 2013.

[12]. M. Frisch, G. W. Trucks, H. B. Schlegel, G. E. Scuseria, M. A. Robb, J. R. Cheeseman, G. Scalmani, V. Barone, B. Mennucci, G. e. Petersson et al., "Gaussian 09 revision d. 01," 2014.

[13]. J. P. Perdew and Y. Wang, "Accurate and simple analytic representation of the electron-gas correlation energy," Physical review B, vol. 45, no. 23, p. 13244, 1992.

[14]. J. P. Perdew, J. A. Chevary, S. H. Vosko, K. A. Jackson, M. R. Pederson, D. J. Singh, and C. Fiolhais, "Atoms, molecules, solids, and surfaces: Applications of the generalized gradient approximation for exchange and correlation," Physical review B, vol. 46, no. 11, p. 6671, 1992.

[15]. M.M. Hasan, M.H. Kabir, M.A. Badsha, M.R. Hossain. A first-principles DFT study on the adsorption behaviour of CO, CO2, and O3 on pristine B24N24 and silicon-decorated B24N24 nanosheet. Phosphorus, Sulfur, and Silicon and the Related Elements. 2021 Oct 2:1-8.

[16]. A. S. Rad and K. Ayub, "O3 and so2 sensing concept on extended surface of b12n12 nanocages modified by nickel decoration: a compre-hensive dft study," Solid State Sciences, vol. 69, pp. 22–30, 2017.

[17]. M. Rezaei-Sameti and N. J. Jukar, "A computational study of nitramide adsorption on the electrical properties of pristine and c-replaced boron nitride nanosheet," Journal of Nanostructure in Chemistry, vol. 7, no. 3, 293–307, 2017.